
[View Journal Online](#)
[View Article Online](#)

Synthesis of nanocellulose/cobalt oxide composite for efficient degradation of Rhodamine B by activation of peroxymonosulfate

 Faouzia Khili ^{1,*} and Amel Dakhlaoui Omrani ²
¹ *Unité de Recherche de Physique des Matériaux Lamellaires et Nanomatériaux Hybrides (PMLNH), Faculté des Sciences de Bizerte, Université de Carthage, 7000 Bizerte, Tunisia*

khilifaouzia@yahoo.fr (F.K.)

² *Laboratoire de Physico-Chimie des Matériaux Minéraux et Leurs Applications, Centre National des Recherches en Sciences des Matériaux, Technopôle de Bordj Cedria, BP73, 8027 Soliman, Tunisia*

dakhlaoui_amel@yahoo.fr (A.D.O.)

 * Corresponding author at: *Unité de Recherche de Physique des Matériaux Lamellaires et Nanomatériaux Hybrides (PMLNH), Faculté des Sciences de Bizerte, Université de Carthage, 7000 Bizerte, Tunisia.*

Tel: +21.65.2640993 Fax: +21.67.2590566 e-mail: khilifaouzia@yahoo.fr (F. Khili).

RESEARCH ARTICLE



doi 10.5155/eurjchem.10.1.19-25.1789

Received: 16 September 2018

Received in revised form: 17 October 2018

Accepted: 20 October 2018

Published online: 31 March 2019

Printed: 31 March 2019

KEYWORDS

 Rhodamine B
 Peroxymonosulfate
 Polymer composites
 Catalytic degradation
 Cellulose monocrystalline
 Cobalt oxide nanoparticles

ABSTRACT

In recent years, nanofibrous materials derived from biopolymers have attracted more interest due to their numerous applications. In our study, a simple composite of cellulose nanocrystals, and cobalt oxide nanoparticles was elaborated using sodium borohydride as a chemical reducer. It has been shown that Co_3O_4 nanoparticles were grown on the surface of cellulose nanocrystals. An important quantity of cobalt oxide nanoparticles was detected using ICP-OES (13.5 g contained in 100 mg of the composite). The size, the morphology and the thermal stability of the composite and the obtained nanoparticles were studied using X-ray powder diffraction, Fourier-transform infrared spectroscopy, Ultraviolet-Visible spectrophotometry, Scanning electron microscopic and Transmission electron microscopic. Our obtained material was used for the degradation of Rhodamine B and it was succeeded in degradation of Rhodamine B within very short period of time (16 min). The catalytic degradation of Rhodamine B was investigated and analyzed with UV-Visible absorption spectra.

 Cite this: *Eur. J. Chem.* 2019, 10(1), 19-25

 Journal website: www.eurjchem.com

1. Introduction

With increasing concern about environmental pollution, scientific researchers turned more to eco-friendly, natural and reusable catalysts. Natural biopolymers, especially cellulose, have been considered as most attractive natural catalysts because of there are inexpensive, biodegradable and could be easily separated and reused.

Cellulose nanocrystals (NCC) are unique nanomaterials derived from the most abundant and almost inexhaustible natural polymer. It is a fibrous, tough, and water insoluble polymer and it plays an essential role in maintaining the structure of plant cell walls. Cellulose presents a wide variety of living species, such as algae, fungi, bacteria and even in some sea animals such as tunicates [1-5]. Nanocellulose is biodegradable, biocompatible, and renewable natural polymer [6-14]. It is considered as an alternate to non-degradable fossil fuel based polymer; it is serving as a sustainable and environmentally friendly material for most applications [15-19]. Innovative applications in diverse fields such as biomedical

engineering, material sciences, electronics, catalysis, etc. where in these cellulose nanocrystals can be used as a fixator of nano-metallic nanoparticles. It can be functionalized with different nanoparticles, to meet various challenging requirements, such as the development of high-performance nanocomposites, using hydrophobic polymer matrices.

In this contribution, we describe a novel method to elaborate a composite of cellulose nanocrystals loaded with cobalt oxide nanoparticles. Cobalt oxide-based materials have been widely used for energy storage system [20], electrochromic thin films [21], magneto resistive devices [22] and heterogeneous catalysis [23]. Cobalt oxides continue to attract considerable attention, mainly due to their excellent electrocatalytic activity to ward various compounds, such as glucose, glutathione, carbohydrate, thiol, hydrogen peroxide, arsenic (III) and methanol [24-29]. Several methods have been developed for the preparation of cobalt oxide including solvothermal process [30], solution spray pyrolysis technique [31] and electrochemical method [32]. Among these techniques, the electrochemical method is an attractive and

promising method. Casella *et al.* have prepared cobalt oxide or oxyhydroxide layers on the surface of gold [33] and glassy carbon electrode [34, 35] by electrodeposition technique [36]. In addition, the electrochemical properties of cobalt oxide films deposited anodically or cathodically at conductive boron doped diamond (BDD) or glassy carbon electrodes have been investigated [37,38]. Polymeric composites containing metal nanoparticles can combine the advantages or distinctive properties of their various constituents

In this work, we report the preparation of cobalt oxide-cellulose nanocrystals composite via in situ synthesis using NaBH_4 as reducing agent. The structure and microstructure of as elaborated materials have been characterized using different techniques. The catalytic properties of as-elaborated nanocomposites were tested against degradation of Rhodamine B.

2. Experimental

2.1. Materials

All chemicals and reagents (Microcrystalline cellulose (< 50 μm , Avicel-101), sulfuric acid, sodium borohydride, cobalt sulfate heptahydrate, peroxymonosulfate (PMS), Rhodamine B (RhB)) used for experiments and analyses were of analytical grade or higher. The water used throughout the experiments was purified with a Milli-Q system from Millipore Co.

2.2. Cellulose nanocrystals preparation

The extraction of cellulose nanocrystals from microcrystalline cellulose (MCC) were performed using acid hydrolysis according to the process described flow: 54 mL of H_2SO_4 (95 %) was added dropwise to dispersed solution of cellulose nanocrystals (5.00 g MCC/50 mL of distilled water). The suspension was heated at 44 °C under constant magnetic stirring for 20 min. The hydrolysis process was stopped by adding cold distilled water. The excess of sulfuric acid was removed by centrifugation at 4000 rpm for 15 min followed by dialysis against ultrapure water using cellulose membrane (12.000-14.000 Daltons) until reaching a constant pH. The suspension was homogenized using a T18 homogenizer (IKA) and dialyzed against Milli-Q water until a constant pH was reached, sonicated for 30 min and freeze-dried during 24 h.

2.3. Preparation of nanocrystalline cellulose/cobalt oxide nanoparticles (NCC/Co₃O₄ NPs) composites

Cobalt oxide nanoparticles loaded nanocrystalline cellulose (NCC/Co₃O₄NPs) nanocomposite was prepared by mixing NCC powder (200 mg) with 20 mL of an aqueous solution of 0.1 M CoSO_4 under stirring for 60 min at room temperature followed by addition of 0.1 M NaBH_4 aqueous solution (20 mL). The precipitate formed after 20 min of continuous magnetic stirring was separated by centrifugation (10 min, 5.000 rpm), washed two times by water then dried in an oven at 50 °C for 12 h.

2.4. Characterization

The UV-Vis absorption spectra were recorded between 200-800 nm using a Perkin Elmer Lambda UV/Vis 950 spectrophotometer and quartz cuvettes with an optical path of 10 mm. Fourier transform infrared (FTIR) spectra were collected using a Thermo Scientific FTIR instrument (Nicolet 8700) at a resolution of 4 cm^{-1} . The pellets used to record the FTIR spectra were prepared by mixing 1mg of dried samples (NCC or NCC/Co₃O₄ NPs) with 99 mg KBr powder in an agate mortar and then pressing into a pellet under load of 7 tons for 2-4 min. The signal from a pure KBr pellet was subtracted as the background. Scanning electron microscopic (SEM) images

were obtained using an electron microscope ULTRA 55 (Zeiss) equipped with a thermal field emitter, three different detectors (EsB detector with filter grid, high efficiency In-lens SE detector, Everhart-Thornley Secondary Electron Detector) and an energy dispersive X-ray analysis device (EDX analysis). Atomic force microscopic (AFM) measurements were performed with a Dimension 3100 Model AFM (Veeco, Santa Barbara, CA) equipped with a Nanoscope IV controller (Digital Instruments) under ambient conditions (relative humidity ~30%, temperature ~22-24 °C). Rectangular single-beam silicon cantilevers (AFM-TM Arrow, Nanoworld) with spring constants of 42 N/m and typical resonant frequencies between 250 and 300 kHz were used. All AFM images were acquired in the tapping mode at a constant force of 5-50 pN. WSxM 5.0 software was used to process images including the local mean plane, profile and roughness measurements. The deposition of NCC on Mica muscovite surface was achieved through drop casting. Transmission electron microscopic (TEM) images were performed with a Philips CM30 microscope operating at 300 kV. The microscope was equipped with a Gatan SS CCD camera and a Digital Micrograph software for the acquisition of electron diffraction patterns, and the dark-field and high-resolution imaging.

2.5. Catalytic activity measurements

The catalytic activity of NCC/Co₃O₄ NPs for the degradation of RhB dye was evaluated in an aqueous solution. The degradation reaction was carried out in a spectrometric quartz cuvette. For the effective degradation of RhB dye, 1 mg (0.5 g/L) of the synthesized NCC/Co₃O₄ NPs catalyst was added into 2 mL aqueous solution of RhB (25 μM) under constant stirring. The suspension was continuously stirred for about 45 min to reach an adsorption-desorption equilibrium between RhB dye and catalyst under dark conditions. Then, 2.4 μL of peroxymonosulfate (0.3 mM) was added to the stable aqueous dye solution under constant stirring. The concentration of RhB was determined using UV-vis spectrophotometry by monitoring the changes in the absorbance maximum at 554 nm.

3. Results and discussion

3.1. Characterization of cobalt cellulose nanocomposites (NCC/Co₃O₄ NPs)

The cellulose nanocrystals/cobalt oxide nanoparticles (NCC/Co₃O₄ NPs) composite was prepared as follow: 200 mg of nanocrystals of cellulose were added to 20 mL of an aqueous solution of cobalt sulfate (0.1 M) then mixed to gather at room temperature under constant magnetic stirring for one hour. The resulting mixture was then reduced using sodium borohydride (NaBH_4 , 0.1 M). The precipitate obtained after 20 min of constant stirring was washed with water and ethanol to eliminate the residue of cobalt sulfate then centrifuged (10 min, 500 rpm) and dried during 12 hour. The black product obtained presents a magnetic characteristics (Figure 1) confirming the presence of cobalt in the final composite. The quantity of cobalt present in the composite was estimated using IC-PES, it was 13.52 g of Co₃O₄ in 100g of the composite.

3.2. Atomic force microscopic measurements of NCC

Figure 2 depicts the AFM image of NCC dispersion drop casted on mica. One clearly sees a single NCC fibre of 400-500 nm in length and 35-40 nm in width.

3.3. SEM and TEM measurements

The SEM and TEM images of the as-elaborated composite (NCC/Co₃O₄) were reported in Figures 3 and 4, respectively.



Figure 1. Easy separation of NCC-Co₃O₄ nanocomposite from an aqueous solution upon application of a magnetic field.

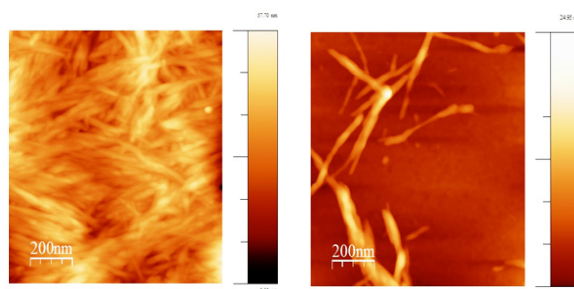


Figure 2. Tapping-mode AFM images of cellulose nanocrystal (NCC) deposited on mica. Additionally, the thickness of the NCC, measured from the line profile as the difference in height between the mica substrate and the fibre, is comprised between 4 and 8 nm.

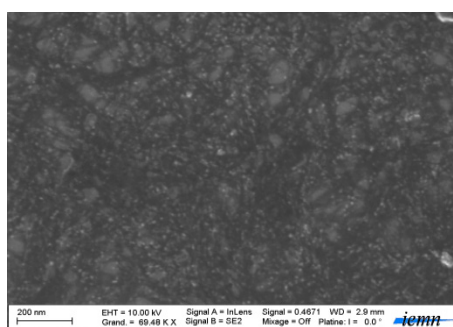


Figure 3. The SEM image of the obtained composite (NCC/Co₃O₄).

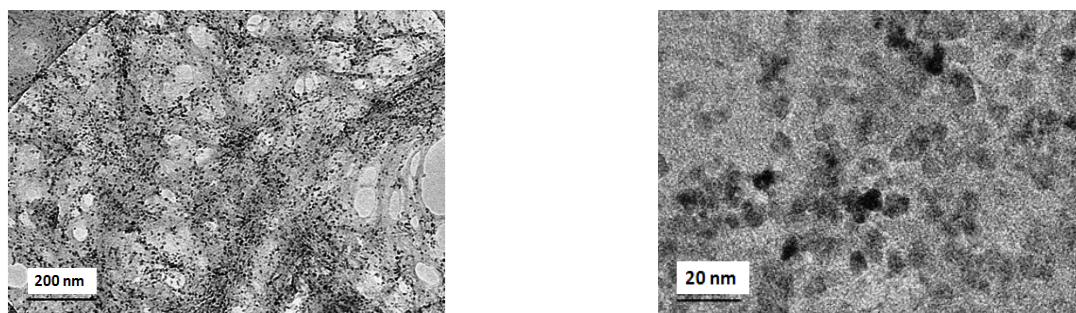


Figure 4. TEM photo of the nanoparticles of cobalt oxide led in the composite (NCC/Co₃O₄).

The SEM images revealed that the sample was formed from extremely fine homogenous sphere-like particles with uniform size of about 15 nm in diameter fixed on the surface of cellulose nanofibers. After the treatments with cobalt sulfates and sodium borohydride, Co₃O₄ NPS were deposited on the surface of the nanofibers of cellulose, indicating successful reduction and aggregate of cobalt ions into metallic Co₃O₄ NPS (Figure 3). However, the average diameter of the led nanoparticles is 5-10 nm. The TEM micrographs confirmed the AFM and SEM observations and show that the nanoparticles are uniform with spherical form.

The EDX pattern (Figure 5) of the as-elaborated composite confirmed the presence of Co, C, present in cellulose and cobalt skeletal.

The composite structure was confirmed using UV-VIS spectroscopy (Figure 6). The same figure shows that the absorbance spectrum of the Co₃O₄ sample with two absorption bands in the range of 250-300 and 40-580 nm wavelength were assigned, respectively, to the O²⁻ → Co²⁺ charge transfer process and to the O²⁻ → Co³⁺ charge transfer [39]. The broad band detected in the range 450 to 550 nm was assigned to the characteristic bands of the cobalt sulfate precursor used in the beginning of the reacted in the reaction.

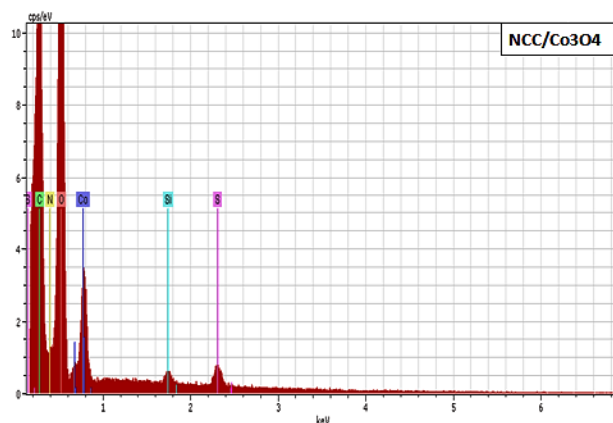


Figure 5. The EDX photo of the composite NCC/Co₃O₄.

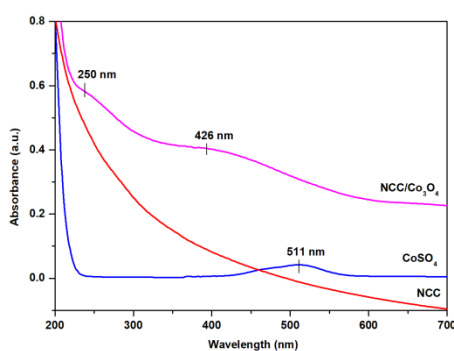


Figure 6. UV-VIS absorption spectra of CoSO₄ (Blue), NCC (red) and NCC-Co₃O₄ nanocomposite (Pink).

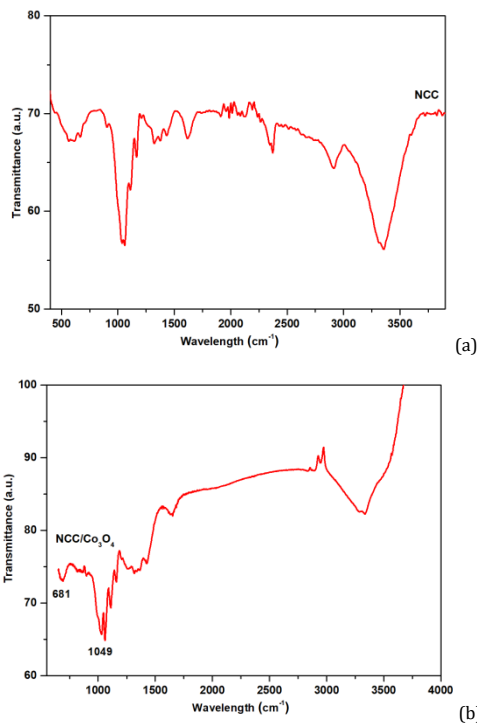


Figure 7. FT-IR spectra of NCC (a) and NCC-Co₃O₄ (b) nanocomposite.

The FT-IR spectra of NCC and NCC-Co₃O₄ are reported in Figure 7. The spectrum of pure NCC shows main bands at 3408, 2928, 1651, 1378 and 1040 cm⁻¹. The broad bands at 3408 and 1040 cm⁻¹ are associated at the stretching vibrations

of hydroxyl (-OH) and C-O groups, respectively. The band at 1651 cm⁻¹ is indicative of intermolecular hydrogen bonds. The peaks at 2928 and 1378 cm⁻¹ are assigned to C-H stretching and bending vibrations, respectively.

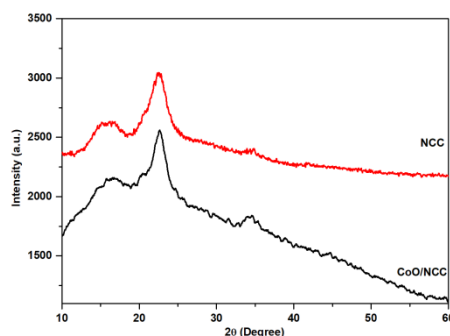


Figure 8. X-ray diffraction (XRD) patterns of nanocrystalline cellulose (NCC) and NCC- Co_3O_4 nanocomposite.

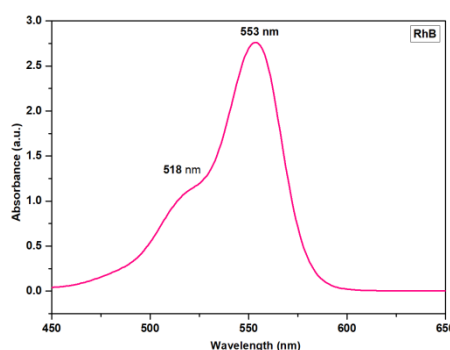


Figure 9. UV-Vis absorption spectra of the initial solution of RhB at $C_0 = 2.5 \times 10^{-6}$ mol/L.

The FT-IR spectra of Co_3O_4 nanoparticles revealed in the region $4000\text{--}500\text{ cm}^{-1}$, showed an absorption bands at 669 cm^{-1} attributed to the stretching vibrations of the metal-oxygen band ($\text{Co}^{3+}\text{--O}$ and $\text{Co}^{2+}\text{--O}$) and confirm the formation of Co_3O_4 spinel oxide [40-43]. Peaks revealed at 1036 and 1110 cm^{-1} were assigned to $\text{Co}\text{--OH}$ vibration [44].

The X-ray diffraction could not be used to characterize the biopolymer cobalt oxide nanocomposite because, due to the large weight fraction of the amorphous polymer matrix (H 90%), the amorphous contribution dominated the scattering spectrum, and it was not possible to clearly discern the metal oxide contribution in the overall scattering of the nanocomposite. We therefore used FT-IR and UV-Vis spectrophotometry to characterize the NCC-cobalt oxide nanocomposite. As shown in XRD diffraction, there is no significant peaks related to cobalt oxide nanoparticles. XRD diffraction showed that the cobalt oxide nanoparticles included in the composite has amorphous or nano-structuralized character as can be seen from Figure 8. The broad peaks can be detected at $2\text{-theta} = 22$ to 34° , related structure of cellulose.

3.4. The degradation of RhB

Recently, many studies were concentrated on the degradation of RhB [45-47]. After the characterization, the composite was used to activate peroxymonosulfate (PMS) for degradation of rhodamine B in aqueous solution. Rhodamine B is a common pollutant existing in industrial wastewater. The catalytic activity of NCC/ Co_3O_4 nanocomposite for the degradation of RhB dye was evaluated in an aqueous solution. The degradation reaction was carried out in a spectrometric quartz cuvette. For the effective degradation of RhB dye, 1 mg (0.5 g/L) of the synthesized NCC/ Co_3O_4 nanocomposite catalyst was added into 2 mL aqueous solution of RhB ($25\text{ }\mu\text{M}$) under constant stirring. The suspension was continuously stirred for about 45 min to reach an adsorption-desorption equilibrium between RhB dye and catalyst under normal

conditions. Then, $2.4\text{ }\mu\text{L}$ of peroxymonosulfate (PMS) (0.3 mM) was added to the stable aqueous dye solution under constant stirring. The concentration of RhB was determined using UV-Vis spectrophotometry by monitoring the changes in the absorbance maximum at 554 nm and a small shoulder at 518 nm (Figure 9).

The catalytic activity of NCC/ Co_3O_4 nanocomposite for the degradation of RhB was examined at room temperature. The course of degradation process was monitored by UV-Vis spectroscopy though the decrease and disappear of peak at 554 nm over the time. This reaction can be followed by the naked eye through color change from pink to transparent.

The degradation of rhodamine B with only PMS was shown in Figure 10, the obtained curves shown that there is no degradation at almost during 1 hour with constant stirring. The Figure 10 shows the degradation of RhB using the prepared catalyst based in cobalt oxide nanoparticles supported nanocellulose (NCC/ Co_3O_4).

The RhB was totally degraded during 16 min . In the obtained curves of the UV-VIS spectrophotometry, we observe that the peak detected at 554 nm , characteristic of RhB was absent after 16 min from addition of catalyst and PMS together. The NCC/ Co_3O_4 /PMS system was very efficient with a full degradation of RhB in less than 16 min at room temperature. The Co_3O_4 composites present a wide pH range for PMS activation. Co^{2+} has been found to possess the highest reactivity. The experimental results suggested that sulfate radicals ($\text{SO}_4^{\cdot-}$) are the main active species in the degradation process. The reusability of heterogeneous catalysts is an important indicator to assess the industrial application potential of heterogeneous catalysts. The NCC/ Co_3O_4 catalyst is stable without any apparent activity loss after 12 cycling runs (Figure 11) [45]. The slight loss of catalytic activity was mainly attributed to the leaching of metal ions during the consecutive runs.

The appropriate mechanism of our system was described below;

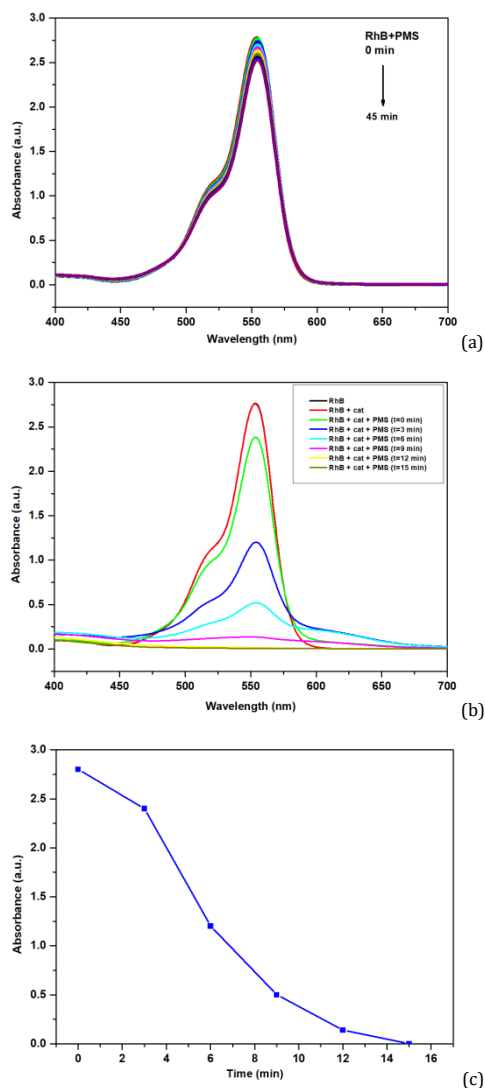


Figure 10. Test of the degradation of RhB with PMS (a), RhB with catalyst and PMS (b), the curve of the decrease of absorbance with time of RhB (c).

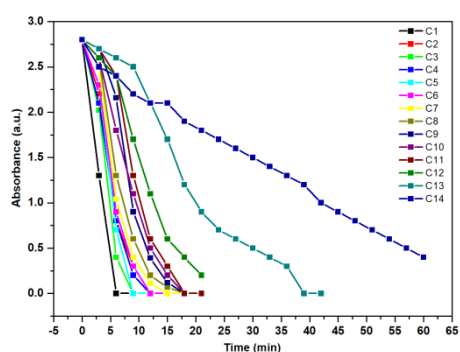
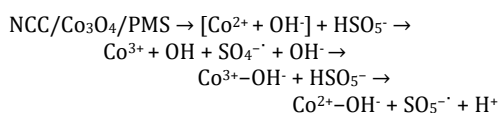
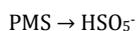
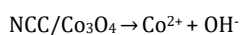


Figure 11. The cycles of reusability of the catalyst (14 cycles).



4. Conclusion

Cobalt oxide nanoparticles loaded on nanocrystalline cellulose were synthesized using a simple chemical process at room temperature by mixing NCC with CoSO_4 salt. This method is simple and does not require the use of any surfactant or reducing agent. Various analytical techniques were used to characterize the nanocomposite. We have demonstrated that the cobalt oxide nanoparticles were

elaborated with size 10 nm as shown in SEM and TEM images. Furthermore, the catalytic activity of the NCC/Co₃O₄ was tested by the degradation of RhB in a simple condition. Thus, this novel synthetic approach for the fabrication of polymer/magnetic nanoparticles holds great potential for advanced catalytic applications.

Disclosure statement

Conflict of interests: The authors declare that they have no conflict of interest.

Author contributions: All authors contributed equally to this work.

Ethical approval: All ethical guidelines have been adhered.

Sample availability: Samples of the compounds are available from the author.

ORCID

Faouzia Khili

 <http://orcid.org/0000-0003-4089-649X>

References

- [1]. Klemm, D.; Heublein, B.; Fink, H. P.; Bohn, A. *Angew. Chem. Int. Ed.* **2005**, *44*, 3358-3393.
- [2]. Sjöström, E. *Wood Chemistry: Fundamentals and applications*, Academic Press Inc., England, 1993.
- [3]. George, J.; Sabapathi, S. N.; Siddaramaiah, Water Soluble Polymer-Based Nanocomposites Containing Cellulose Nanocrystals. In: Thakur V., Hakur M. (eds) *Eco-friendly Polymer Nanocomposites. Advanced Structured Materials*, vol. 75, pp. 259-293, Springer, New Delhi, 2015.
- [4]. Eichhorn, S. J.; Baillie, C. A.; Zafeiropoulos, N.; Mwaikambo, L. Y.; Ansell, M. P.; Dufresne, A.; Entwistle, K. M.; Herrera-Franco, P. J.; Escamilla, G. C.; Groom, L. H.; Hughes, M.; Hill, C.; Rials, T. G.; Wild, P. *M. J. Mater. Sci.* **2001**, *36*, 2107-2131.
- [5]. Masaoka, S.; Ohe, T.; Sakota, N. *J. Ferment. Bioeng.* **1993**, *75*, 18-22.
- [6]. Habibi, Y.; Lucia, L. A.; Rojas, O. *J. Chem. Rev.* **2010**, *110*, 3479-3500.
- [7]. Ahmad, N.; Wahab, R.; Al-Omar, S. *Eur. J. Chem.* **2014**, *5(2)*, 247-251.
- [8]. Moon, R. J.; Martini, A.; Nairn, J.; Simonsen, J.; Young, B. *J. Chem. Soc. Rev.* **2011**, *40*, 3941-3994.
- [9]. Iwamoto, S.; Kai, W.; Isogai, A.; Iwata, T. *Biomacromol.* **2009**, *10*, 2571-2576.
- [10]. Lahiji, R. R.; Xu, X.; Reifemberger, R.; Raman, A.; Rudie, A.; Moon, R. J. *Langmuir* **2010**, *26*, 4480-4488.
- [11]. Sturcova, A.; Davies, G. R.; Eichhorn, S. J. *Biomacromol.* **2005**, *6*, 1055-1061.
- [12]. Revol, J. F.; Bradford, H.; Giasson, J.; Marchessault, R. H.; Gray, D. G. *Int. J. Biol. Macromol.* **1992**, *14*, 170-172.
- [13]. Orts, W. J.; Godbout, L.; Marchessault, R. H.; Revol, J. F. *Macromol.* **1998**, *31*, 5717-5725.
- [14]. Azizi, S.; Alloin, F.; Sanchez, J. Y.; El Kissi, N.; Dufresne, A. *Macromol.* **2004**, *37*, 1386-1393.
- [15]. Araki, J.; Wada, M.; Kuga, S.; Okano, T. *J. Wood Sci.* **1999**, *45*, 258-261.
- [16]. Romany, M.; Shuping, D.; Hirani, A.; Yong, W. L. ACS symposium series. Vol. 1017. Oxford University Press, Cellulose nanocrystals for drug delivery; pp. 81-91, 2009.
- [17]. Lam, E.; Male, K. B.; Chong, J. H.; Leung, A. C.; Luong, J. H. *Trends Biotechnol.* **2012**, *30*, 283-290.
- [18]. Taheri, A.; Mohammadi, M. *Chem. Biol. Drug. Des.* **2015**, *86*, 102-106.
- [19]. Jackson, J. K.; Letchford, K.; Wasserman, B. Z.; Ye, L.; Hamad, W. Y.; Burt, H. M. *Int. J. Nanomedic.* **2011**, *6*, 321-330.
- [20]. Kandalkar, S. G.; Dhawale, D. S.; Kim, C. K.; Lokhande, C. D. *Synth. Met.* **2010**, *160*, 1299-1302.
- [21]. Yoshino, T.; Baba, N. *Sol. Energ. Mat. Sol. C* **1995**, *39*, 391-397.
- [22]. Okabe, H.; Akimitsu, J.; Kubodera, T.; Matoba, M.; Kyomen, T.; Itoh, M. *Phys. B Condens. Matter.* **2006**, *378-380*, 863-864.
- [23]. Rashkova, V.; Kitora, S.; Konstantinov, I.; Vitahov, T. *Electrochim. Acta* **2002**, *47*, 1555-1560.
- [24]. Ding, Y.; Wang, Y.; Su, L.; Bellagamba, M.; Zhang, H.; Lei, Y. *Biosens. Bioelectron.* **2010**, *26*, 542-548.
- [25]. Buratti, S.; Brunetti, B.; Mannino, S. *Talanta* **2008**, *76*, 454-457.
- [26]. Xia, Y. S.; Dai, H. X.; Jiang, H. Y.; Zhang, L. *Catal. Commun.* **2010**, *11*, 1171-1175.
- [27]. Hou, Y.; Ndamani, J. C.; Guo, L. P.; Peng, X. J.; Bai, J. *Electrochim. Acta* **2009**, *54*, 6166-6171.
- [28]. Salimi, A.; Hallaj, R.; Soltanian, S.; Mamkhezri, H. *Anal. Chim. Acta* **2007**, *594*, 24-31.
- [29]. Salimi, A.; Mamkhezri, H.; Hallaj, R.; Soltanian, S. *Sens Actuators B* **2008**, *129*, 246-254.
- [30]. Qi, Y. C.; Zhao, Y. B.; Wu, Z. S. *Mater. Chem. Phys.* **2008**, *110*, 457-462.
- [31]. Shinde, V. R.; Mahadik, S. B.; Gujar, T. P.; Lokhande, C. D. *Appl. Surf. Sci.* **2006**, *252*, 7487-7492.
- [32]. Xia, X. H.; Tu, J. P.; Xiang, J. Y.; Huang, X. H.; Wang, X. L.; Zhao, X. B. *Power Sources* **2010**, *195*, 2014-2022.
- [33]. Casella, I. G.; Guascito, M. R. *Electroanal. J. Chem.* **1999**, *476*, 54-63.
- [34]. Casella, I. G.; Gatta, M.; *Electro. Anal. Chem.* **2002**, *534*, 31-38.
- [35]. Casella, I. G. *J. Electroanal. Chem.* **2002**, *520*, 119-125.
- [36]. Hao, M.; Pegah, K.; Foro, S.; Pratik, U. J.; Julie, O.; Xue, M.; Christa, M.; Rattapol, P.; Jonathan, K.; Ameya, N.; Weilue, H. M.; Frost, C.; Heldt, C. H.; Lee, B. P. *Acta Biomaterialia* **2019**, *83*, 109-118.
- [37]. Spataru, N.; Terashima, C.; Tokuhiko, K.; Sutamto, I.; Tryk, D. A.; Park, S. M.; Fujishima, A. *J. Electrochem. Soc.* **2003**, *150*, 337-334.
- [38]. McNally, E. A.; Zhitomirsky, I.; Wilkinson, D. S. *Mater. Chem. Phys.* **2005**, *91*, 391-398.
- [39]. Figgis, B. N. *Introduction to Ligand Fields*, Interscience, New York, London, Sydney, 1996.
- [40]. Faouzia, K.; Joao, B.; Pedro, L. A.; Rabah, B.; Amel, D. O. *Waste Biomass. Valori.* **2018**, *18*, 1-15.
- [41]. Windisch, C. F.; Exarhos, G. J.; Owings, R. R. *J. Appl. Phys.* **2004**, *95*, 5435-5442.
- [42]. Navale, S. T.; Liu, C.; Gaikar, P.; Patil, V.; Sagar, R. U. R.; Du, B.; Mane, R. S.; Staler, F. *Sens. Actuators B Chem.* **2017**, *245*, 524-532.
- [43]. Zhou, T.; Lu, P.; Zhang, Z.; Wang, Q.; Umar, A. *Sens. Actuators B Chem.* **2016**, *235*, 457-465.
- [44]. Makhlof, M. T.; Abu-Zied, B. M.; Mansoure, T. H. *Fuel J. Nanopart.* **2013**, *2013*, 1-7.
- [45]. Monaam, B. A.; Alexandre, B.; Ahmed, A.; Brigitte, S.; Habib, E.; Mokhtar F.; Sabine, S.; Rabah, B. *Phys. Chem. Chem. Phys.* **2017**, *19*, 6569-6578.
- [46]. Akir, S.; Abderrahmane, H.; Ahmed, A.; Yannick, C.; Rabah B.; Amel, D. O. *Appl. Surf. Sci.* **2017**, *400*, 461-470.
- [47]. Abdel-Hady, A. *Eur. J. Chem.* **2013**, *4(3)*, 292-296.



Copyright © 2019 by Authors. This work is published and licensed by Atlanta Publishing House LLC, Atlanta, GA, USA. The full terms of this license are available at <http://www.eurjchem.com/index.php/eurjchem/pages/view/terms> and incorporate the Creative Commons Attribution-Non Commercial (CC BY NC) (International, v4.0) License (<http://creativecommons.org/licenses/by-nc/4.0>). By accessing the work, you hereby accept the Terms. This is an open access article distributed under the terms and conditions of the CC BY NC License, which permits unrestricted non-commercial use, distribution, and reproduction in any medium, provided the original work is properly cited without any further permission from Atlanta Publishing House LLC (European Journal of Chemistry). No use, distribution or reproduction is permitted which does not comply with these terms. Permissions for commercial use of this work beyond the scope of the License (<http://www.eurjchem.com/index.php/eurjchem/pages/view/terms>) are administered by Atlanta Publishing House LLC (European Journal of Chemistry).